Macromolecular Rapid Communications
www.mrc-journal.de

Revisiting the Classical Wide-Bandgap Homo and Random Copolymers for Indoor Artificial Light Photovoltaics

Jeonga Kim, Muhammad Ahsan Saeed, Sung Hyun Kim, Dongmin Lee, Yongchan Jang, Jin Su Park, Donggu Lee, Changyeon Lee, Bumjoon J. Kim, Han Young Woo, Jae Won Shim, and Wonho Lee**

Organic indoor photovoltaics (IPVs) are attractive energy harvesting devices for low-power consumption electronic devices and the Internet of Things (IoTs) owing to their properties such as being lightweight, semitransparent, having multicoloring capability, and flexibility. It is important to match the absorption range of photoactive materials with the emission spectra of indoor light sources that have a visible range of 400–700 nm for IPVs to provide sustainable, high-power density. To this end, benzo[1,2-b:4,5-b′]dithiophene-based homopolymer (PBDTT) is synthesized as a polymer donor, which is a classical material that has a wide bandgap with a deep highest occupied molecular orbitals (HOMO) level, and a series of random copolymers by incorporating thieno[3,4-c]pyrrole-4,6,-dione (TPD) as a weak electron acceptor unit in PBDTT. The composition of the TPD unit is varied to fine tune the absorption range of the polymers; the polymer containing 70% TPD (B30T70) perfectly covers the entire range of indoor lamps such as light-emitting diodes (LEDs) and fluorescent lamp (FL). Consequently, B30T70 shows a dramatic enhancement of the power conversion efficiency (PCE) from 1-sun (PCE: 6.0%) to the indoor environment (PCE: 18.3%) when fabricating organic IPVs by blending with $PC_{71}BM$. The simple, easy molecular design guidelines are suggested to develop photoactive materials for efficient organic IPVs.

1. Introduction

One of the key challenges for realizing the Internet of Things (IoTs), which connects billions of Internet-enabled smart devices and sensors into the IoT network, is to develop energy harvesting devices that can act as alternatives or work in conjunction with batteries; although the energy densities of batteries have increased greatly over the last few decades, they have a limited lifetime along with the need for periodic charge and maintenance (or replacement).[1–5] Various indoor energy harvesters with power in the range of 1–100 μW, which includes piezoelectric and triboelectric generators using mechanical energy, thermoelectric generators using waste heat, ratchets using radiofrequency, and indoor light photovoltaics (IPVs) have been proposed because autonomous IoTs are located inside buildings.[1,5–10] Among them, IPVs are a promising candidate for addressing these challenges; they can supply reliable energy inside buildings with good predictability and controllability.[5,11–13] Organic photovoltaics (OPVs), in which the

J. Kim, D. Lee, Y. Jang, W. Lee
Department of Polymer Science and Engineering
Department of Energy Engineering Convergence
Kumoh National Institute of Technology
Gumi, Gyeongbuk 39177, Republic of Korea
E-mail: 1holee@kumoh.ac.kr

M. A. Saeed
Division of Electronics and Electrical Engineering
Dongguk University
Seoul 04620, Republic of Korea

S. H. Kim, J. W. Shim
School of Electrical Engineering
Korea University
Seoul 02841, Republic of Korea
E-mail: jwshim19@korea.ac.kr

The ORCID identification number(s) for the author(s) of this article can be found under https://doi.org/10.1002/marc.202200279

DOI: 10.1002/marc.202200279

J. S. Park, B. J. Kim
Department of Chemical and Biomolecular Engineering
Korea Advanced Institute of Science and Technology (KAIST)
Daejeon 34141, Republic of Korea

D. Lee
Department of Semiconductor Engineering
Gyeongsang National University
Jinju, Gyeongsangnam-do 52828, Republic of Korea

C. Lee
Department of Chemical and Biomolecular Engineering
University of Pennsylvania
Philadelphia, PA 19104, USA

H. Y. Woo
Department of Chemistry
College of Science
Korea University
Seoul 02841, Republic of Korea

photoactive layers comprise organic conjugated polymers (or small molecules), establish their superiority because of their cost-effectiveness, high transparency, facile fabrication processes, reduced environmental risks, high optical absorption in the visible region, tunable energy levels, and robust mechanical endurance.[14–17] In particular, the very thin film nature of OPVs with total thicknesses less than 500 nm and the tunable optical bandgap (E_g) of photoactive materials with vivid colors makes them more attractive for use inside buildings; we believe that most people may not want to install conventional Si-based photovoltaics in their own houses.

In the last few decades, OPVs have experienced rapid progress via the optimization of photoactive donor acceptor materials and device engineering with an understanding of device physics.[18–24] For designing photoactive materials, extensive research has focused on synthesizing low-bandgap donor/acceptor materials that can cover the ultraviolet, visible, and infrared regions of solar irradiation to maximize photocurrent generation.[25–28] However, the scenario changes when considering the indoor environment. The emission spectra of indoor lighting sources such as light-emitting diodes (LEDs) and fluorescent lamps (FL) are restricted to the visible wavelength region (400–700 nm), and their light levels are significantly reduced to less than 1000 lx, which requires different molecular design strategies for efficient organic IPVs.[3,29–31] When bringing OPVs that are specifically optimized under AM 1.5G illumination into the indoor environment, which usually have an absorption edge of 700–900 nm, it is unavoidable to have energy loss (E_{loss}) induced by the absorption behavior beyond 700 nm.[30,32] Therefore, it is of utmost importance to design photoactive materials spectrally matched with the indoor lighting sources; otherwise, we have no chance to reach the theoretical maximum (≈57%) of the power conversion efficiencies (PCEs) of organic IPVs.[33] Cui et al. successfully demonstrated the importance of spectral matching by designing wide-bandgap nonfullerene acceptors (NFAs) of IO-4Cl (E_g = 1.8 eV).[30] The PBDB-TF (polymer):IO-4Cl (NFA) blend has an absorption range of 400–700 nm, and it is perfectly matched with the LEDs they used; therefore, a high PCE of 26.1% under LEDs (1000 lx) was achieved with low E_{loss}. We note that the PCE under the standard AM 1.5G conditions was only 9.80%. Lee et al. also reported highly efficient organic IPVs using a blend of small molecule donor (BTR) and $PC_{71}BM$.[14] The absorption range of blend film efficiently covers FL (1000 lx) they used, and a high PCE of 28.1% was recorded; this blend also showed moderate PCE of 10.5% under the standard AM 1.5G conditions. In addition, Ma et al. reported PCE over 30% using polymer donor PM6 with NFA (Y6-O).[17] They optimized electron transport layer (ETL) to reduce leakage current and trap-assisted recombination under low light levels, then PCEs of 29.5, 30.0, and 30.9% were achieved under LEDs of 700, 1200, and 1650 lx, respectively.

To design wide-bandgap donor materials for organic IPVs, we revisit classical homopolymers, which have a wide E_g because of the absence of intramolecular charge transfer; thus far, most researchers do not focus on these materials over the past decade. Homopolymers have an obvious advantage in terms of the time and cost-effectiveness for synthesis because of their simple chemical structures. Among the various homopolymers reported so far, benzodithiophene-based homopolymers are promising candidates for polymer donors in organic IPVs because they have a deep highest occupied molecular orbital (HOMO) level affordable to a high open-circuit voltage (V_{OC}). In 2015 and 2016, poly(4,8-bis(5-(2-ethylhexyl)thiophene-2-yl)benzo[1,2-b:4,5-b']dithiophene) (PBDTT) was reported by two groups; the polymer has a HOMO level around −5.4 eV, and the moderate PCE of 6.12% with a high V_{OC} over 0.9 V under the standard AM 1.5G conditions recorded when blended with $PC_{71}BM$.[34,35] The results are interesting because there have been almost no reports on successful homopolymers that show a comparable or higher photovoltaic performance than that of the well-known poly(3-hexylthiophene) (P3HT) homopolymer. However, when considering the introduction of PBDTT into organic IPVs, it has an excessively wide E_g (2.13 eV) with an absorption edge below 600 nm. Therefore, photons of 600–700 nm emitted from LEDs or FL are transparent to PBDTT, which requires further chemical engineering for spectral matching with indoor lighting sources.

We aim to fine tune the absorption range of PBDTT homopolymers while maintaining their high V_{OC} via random copolymerization strategies. We simply introduced thieno[3,4-c]pyrrole-4,6-dione (TPD) as the second monomer into PBDTT to afford PBDTT-TPD random copolymers for covering the emission spectra of 600–700 nm in LEDs and FL. The TPD has a weak electron acceptor nature, and therefore, it is possible to red-shift the absorption range without sacrificing the V_{OC}. Absorption properties were easily controlled by varying the ratios of BDTT and TPD units; we found that the random copolymer with 30% BDTT and 70% TPD compositions (B30T70) perfectly covered the entire range of LEDs and FL, which resulted in a PCE of 18.3% when blended with $PC_{71}BM$ under FL 1000 lx. We note that B30T70:$PC_{71}BM$ exhibited moderate PCE under AM 1.5G illumination (only 6.0%), which means that significant increment over three times was achieved from 1-sun to indoor light conditions. Our findings suggest that organic IPV communities should revisit classical wide-bandgap photoactive materials to produce efficient organic IPVs via a slight chemical modification of them, although they may have underperformed under AM 1.5G conditions.

2. Results and Discussion

2.1. Synthesis of Indoor Light Matched Donor Polymers Based on the PBDTT Homopolymer

Figure 1a presents the chemical structure and absorption spectrum of the wide-bandgap homopolymer (PBDTT), wherein the normalized spectra of AM 1.5G and the most commonly used indoor light sources (LED and FL) are included. The PBDTT homopolymer has obvious advantages of easy synthesis and a deep HOMO level; therefore, it holds the potential for applications in indoor photovoltaics as donor polymers considering time- and cost-effectiveness. However, the absorption range of PBDTT is not perfectly matched with the LED and FL spectra; a large number of photons (600–700 nm) are transparent to PBDTT (Figure 1a). In this regard, we introduce a second TPD moiety that can possibly extend the absorption range to ≈700 nm to match the indoor light spectra of both LED and FL.[36–38]

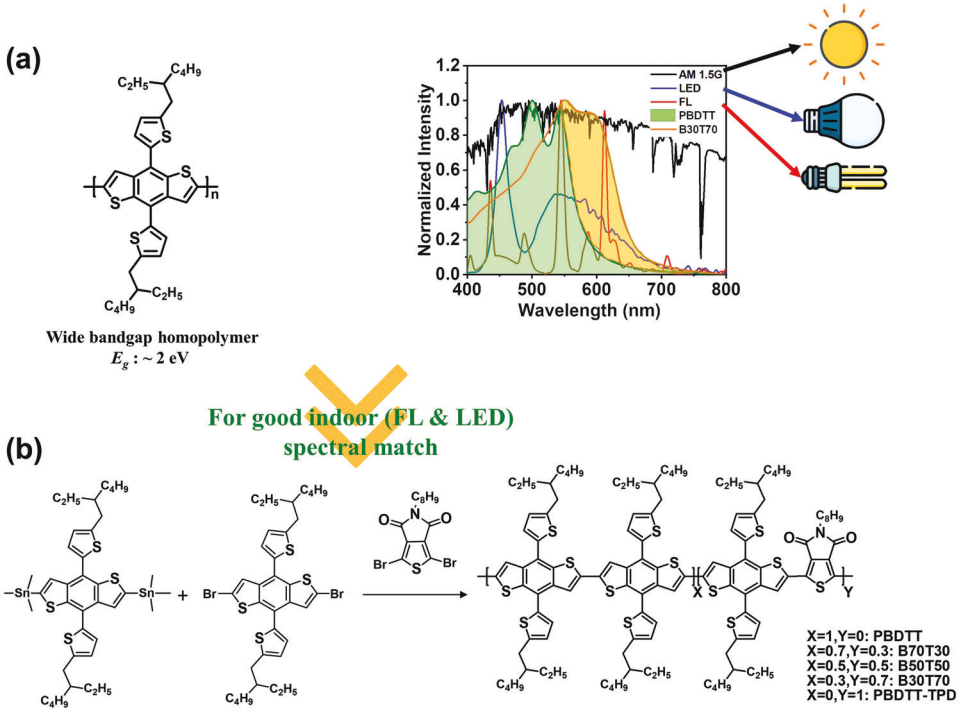

Figure 1. a) Chemical structure and absorption spectrum of homopolymer (PBDTT) with a spectra of AM 1.5G and the most common indoor light sources (light-emitting diode [LED] and fluorescent lamp [FL]); green and orange area indicate the absorption ranges of homopolymer (PBDTT) and the additional absorption of random copolymer (B30T70), respectively. b) Synthetic routes of five different polymers.

Table 1. Molecular weights, thermal, electrochemical, and optical properties of the polymers.

Polymerdonors	M_n [kg mol^{-1}] [a]	$Đ$ (M_w/M_n) [a]	T_d [°C] [b]	λ_{max}^{neat} [nm] [c]	λ_{onset}^{neat} [nm] [c]	E_g^{opt} [eV] [d]
PBDTT	16.6	1.92	418	500, 542	600	2.07
B70T30	16.1	4.33	407	507, 547	636	1.94
B50T50	16.2	2.65	417	547	653	1.90
B30T70	16.9	3.87	431	547, 590	670	1.85
PBDTT-TPD	14.8	3.18	430	557, 613	677	1.83

[a] determined by size exclusion chromatography (SEC) with polystyrene standard;[34] [b] determined by thermogravimetric analysis (TGA; 5% weight loss); [c] polymer films on glass substrates by spin casting from a chloroform solution at 1000 rpm for 60 s; [d] calculated from the absorption edge in the film state.

Figure 1b shows the synthetic routes to five different polymers, which includes the PBDTT homopolymer, PBDTT-TPD alternating copolymer, and random copolymers. We varied the contents of the TPD moiety from 30% (B70T30), 50% (B50T50), and 70% (B30T70) to examine the effect of adding a TPD moiety to the PBDTT homopolymer on the performance of indoor photovoltaics; change in the absorption range is the main property by introducing TPD moiety as shown in green (absorption of PBDTT) and orange area (the additional absorption of random copolymer B30T70) of Figure 1a, which will be discussed in detail. All polymers were synthesized via the Stille coupling reaction using stannylated BDTT with brominated BDTT and/or TPD monomers in a microwave reactor.[34,38,39] Detailed synthesis procedures and yields are stated in Experimental Section. The number average molecular weights (M_n) and dispersity ($Đ$) of polymers were estimated by size exclusion chromatography (SEC) with *o*-dichlorobenzene as the eluent. As summarized in **Table 1**, all polymers exhibited similar M_n values of 14.0–17.0 kg mol^{-1} but having different dispersity ($Đ$). The chemical structures of polymers were confirmed by ^{1}H NMR spectroscopy in 1,2-dichlorobenzene-d_4 solution at 75 °C (Figures S1–S5, Supporting Information). We also calculated the actual ratios between BDTT and TPP in random copolymers by elemental analysis (Table S1, Supporting Information). Overall, all random copolymers exhibited slightly lower TPD contents than those of monomer feed ratios, but the difference is not significant.

Thermogravimetric analysis (TGA) and differential scanning calorimetry (DSC) were used to evaluate the thermal properties of the polymers. As shown in Figure S6 (Supporting Information) of the TGA curves, all polymers are highly stable with a decomposition temperature (T_d) above 400 °C (Table 1). Introducing a TPD moiety into PBDTT homopolymers does not adversely affect the thermal stability of the polymers. Figure S7 (Supporting Information) presents the second heating and cooling curves of the

DSC, which shows no thermal transition from 50 °C to 300 °C. All polymers had an amorphous nature.

2.2. Optical and Electrochemical Properties

The optical and electrochemical properties of polymer donors are important for improving their photovoltaic performance under AM 1.5G and indoor light. We measured the UV-vis absorption spectra of polymers in the solution and film states to investigate how different TPD contents affect the absorption behavior of the polymers (Figure S8, Supporting Information and **Figure 2**). As shown in Figure 2a of UV-vis absorption spectra in films, the absorption ranges are broadened and red-shifted with an increase in TPD contents. This is because the electron-deficient TPD moiety enhances the pull-push effects, which reduce the optical bandgap (E_g^{opt}) of the polymers.[40] We summarize E_g^{opt} of the polymers in Table 1, which are estimated from the absorption onsets of the polymers, and it decreased from 2.07 eV of PBDTT homopolymer to 1.94–1.85 eV of random copolymers (B70T30 – B30T70). Interestingly, introducing the TPD moiety to the PBDTT homopolymer solves the weak point of the PBDTT homopolymer that does not absorb the main irradiance peak of FL (611 nm). When a small amount of TPD moiety (30%) was introduced, it started to cover 611 nm of the FL. Then, the B30T70 random copolymer perfectly absorbs the entire range of FL because the TPD content further increased to 70%; PBDTT-TPD also covers the FL. Further, we measured the UV-vis absorption spectra of the blend films of polymer:$PC_{71}BM$ (Figure 2b). The main absorption of $PC_{71}BM$ is located at 400–600 nm, and it has complementary absorption with donor polymers located in the range of 500–700 nm. Therefore, the blend films of B30T70 and PBDTT-TPD effectively absorb the entire range of the FL indoor light, of which the blends can exhibit high-performance IPVs; this will be discussed later. The absorption spectra in dilute chlorobenzene solution were also measured under different temperature to investigate macromolecular aggregation behavior. As shown in Figure S8b–f (Supporting Information), all polymers have similar absorption behavior: absorption intensities at the longer wavelength were slightly decreased as increasing the temperature of polymer solutions. It seems that B30T70 and PBDTT-TPD exhibit more decreased absorption intensities compared to other polymers, but the difference is not significant. Therefore, all polymers have similar aggregation behavior in dilute solution state.

The HOMO energy levels were measured by cyclic voltammetry (CV) (Figure S9, Supporting Information). Figure 2c depicts the HOMO and lowest unoccupied molecular orbital (LUMO) energy levels of polymers and $PC_{71}BM$. The PBDTT homopolymer already has a deep HOMO energy level of −5.44 eV. Notably, the values get deeper when only 30% TPD was introduced, which is almost similar to that of PBDTT-TPD: −5.61 eV (B70T30), −5.62 eV (B50T50), −5.64 eV (B30T70), and −5.62 eV (PBDTT-TPD). This is because the frontier energy levels of push-pull polymers can be saturated at relatively short repeating units.[41] All random copolymers can show high open-circuit voltage (V_{OC}) comparable to the alternating copolymer of PBDTT-TPD.[42] Further, deeper HOMO energy levels and a wider absorption of polymers containing the TPD moiety are beneficial for reducing energy loss.[30,32] All polymers have sufficient LUMO offsets of more than 0.3 eV with $PC_{71}BM$, which is suitable for the photoinduced charge transfer between donors and acceptors.[43]

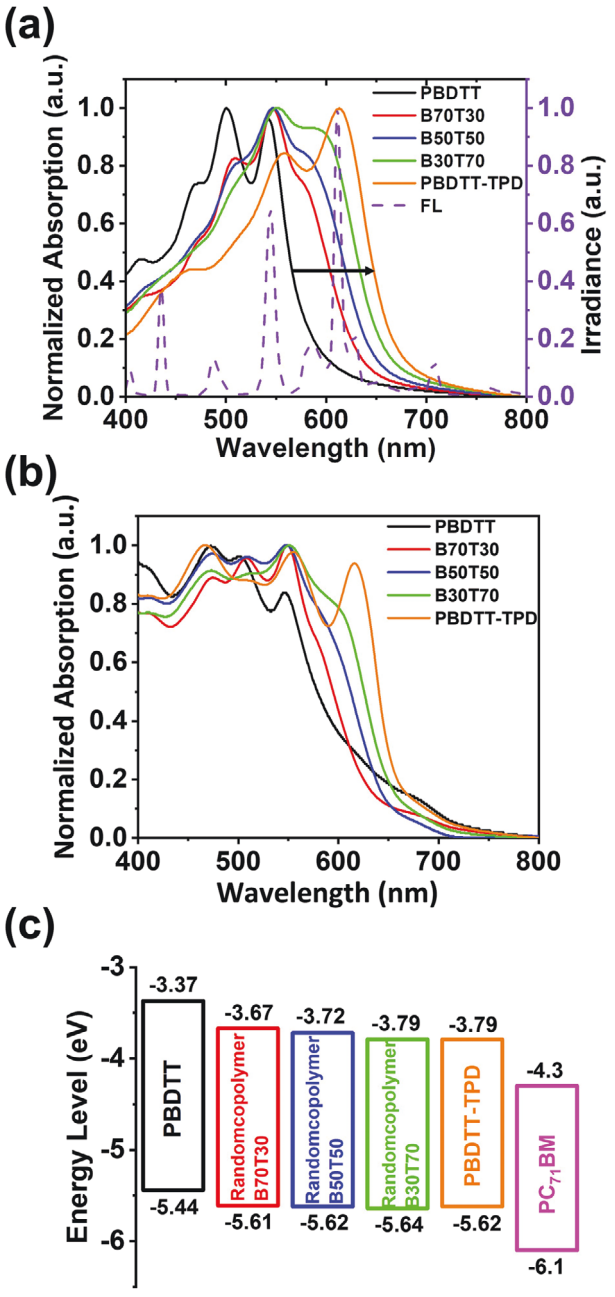

Figure 2. a) UV-vis absorption spectra of pristine polymer films with the emission spectra of fluorescent lamp (FL) and b) donor:acceptor blend film. c) Energy levels of PBDTT, PBDTT based random copolymers, PBDTT-TPD, and $PC_{71}BM$.

2.3. Photovoltaic Performance Under AM 1.5G

The effect of the random copolymer strategy on the photovoltaic performance of the devices was examined by fabricating OPVs in an inverted structure with the configuration of ITO/ZnO/PEIE/polymer blend/MoO_x/Ag. The employment of

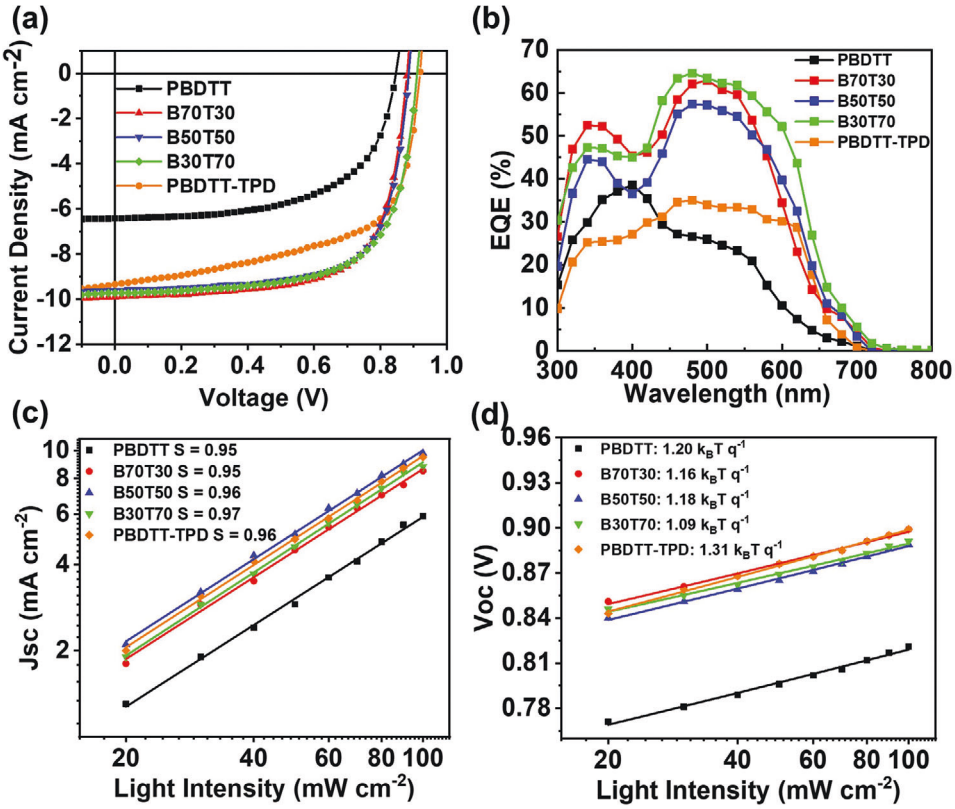

Figure 3. Photovoltaic performance of devices under AM 1.5G. a) *J–V* curves and b) external quantum efficiency (EQE) spectra. Variation in c) J_{SC} and (d) V_{OC} dependencies of light intensity for photovoltaics.

Table 2. Photovoltaic properties under AM 1.5G, SCLC mobilities, and series/shunt resistance.

Active layer	V_{OC} [V]	J_{SC} [mA cm^{-2}]	FF [%]	PCE [%]	$\mu_h^{pristine}$ [cm^2 V^{-1} s^{-1}]	μ_h^{blend} [cm^2 V^{-1} s^{-1}]	μ_e^{blend} [cm^2 V^{-1} s^{-1}]	μ_h/μ_e	R_s [Ω cm^2]	R_{sh} [Ω cm^2]
PBDTT	0.84 ± 0.01	6.1 ± 0.2	57.4 ± 1.7	3.0 ± 0.1	1.38×10^{-4}	1.10×10^{-5}	1.85×10^{-5}	0.595	3.16	2069
B70T30	0.89 ± 0.01	10.0 ± 0.2	71.9 ± 0.4	6.4 ± 0.1	3.93×10^{-4}	2.36×10^{-6}	2.68×10^{-6}	0.881	4.21	2045
B50T50	0.90 ± 0.01	9.6 ± 0.1	70.7 ± 0.9	6.1 ± 0.1	2.42×10^{-4}	1.33×10^{-6}	4.98×10^{-6}	0.267	3.89	1730
B30T70	0.91 ± 0.01	9.9 ± 0.2	67.0 ± 0.8	6.0 ± 0.1	4.56×10^{-4}	2.40×10^{-6}	4.54×10^{-6}	0.529	5.98	2195
PBDTT-TPD	0.91 ± 0.01	9.4 ± 0.2	58.1 ± 2.1	4.9 ± 0.3	1.70×10^{-3}	1.58×10^{-6}	1.51×10^{-5}	0.105	6.94	504

the inverted structure with the MoO_x/Ag top charge collecting electrodes (CCEs) enhances device stability in comparison to that of the conventional structure with Ca/Al CCEs.[44,45] The current density versus voltage (*J–V*) characteristic curves of OPV devices under AM 1.5G illumination at an intensity of 100 mW cm^{-2} are illustrated in **Figure 3**a and in the dark in Figure S10 (Supporting Information). Photovoltaic parameters of devices are summarized in **Table 2**. The PCEs of our blend systems are not impressive as compared to state-of-the-art OPVs; the aim of our study is not the development of photoactive materials for high performance OPVs. We want to highlight the importance of spectral match for producing efficient IPVs by revisiting classical wide bandgap materials.

OPV devices with the PBDTT polymer showed the lowest PCE of 3.0% with a V_{OC} of 0.84 V, J_{SC} of 6.1 mA cm^{-2}, and fill factor (FF) of 57.0%. The significantly low values of short-circuit current density (J_{SC}) can be attributed to the narrow absorption window of PBDTT (Figure 2). Further, PBDTT homopolymers have poor solubility compared to others, which contributes to the performance degradation of PBDTT-based OPVs. Random copolymers exhibited PCEs of 6.4%, 6.1%, and 6.0% (twofolds higher than PBDTT homopolymer) with corresponding V_{OC} values of 0.89, 0.90, and 0.91 V, J_{SC} values of 10.0, 9.6, 9.9 mA cm^{-2}, and FF values of 71.9%, 70.7%, and 67.0% for B70T30-, B50T50-, and B30T70-based devices, respectively. The better performance of random copolymer devices can be attributed to the substantial improvement in the J_{SC} and FF values. Although PBDTT-TPD possesses good absorption properties such as random copolymers, devices with the PBDTT-TPD polymer resulted in a relatively low PCE of 4.9% with a V_{OC} of 0.91 V, J_{SC} of 9.4 mA cm^{-2},

and FF of 58.1%. The FF values of PBDTT-TPD polymer significantly decrease because of the higher series resistance (R_s) and lower shunt resistance (R_{sh}) than other polymers (Table 2). A detailed discussion will be provided in the section on the charge carrier and morphological properties. The relatively high V_{OC} values of PBDTT-TPD and random copolymers ranging from approximately 0.89 to 0.91 V can be attributed to their deep HOMO levels (≈5.6 eV) because the V_{OC} is linearly proportional to the energy level difference between polymer donor (HOMO) and acceptor (LUMO). The V_{OC} values of PBDTT are slightly low (≈0.84 V) because of its high HOMO level (≈5.4 eV). The difference in the J_{SC} values of the devices was further evaluated by measuring the external quantum efficiency (EQE) spectra (Figure 3b). The J_{SC} improvement in the random copolymer devices matches well with the modification in their spectral response in the EQE spectra. The significantly low value of the measured J_{SC} in PBDTT is consistent with the poor EQE curve. The EQE values of random copolymers were considerably higher than those of PBDTT-TPD and PBDTT over the entire visible wavelength range. The maximum EQE values of the B30T70 and B70T30 polymers were measured to be as high as ≈65% and ≈63% at wavelengths of 490 and 500 nm, respectively. In addition, different molecular weights of polymers can affect photovoltaic performance. It is considered that high molecular weight polymers usually produce excellent photovoltaic performances.[46–48] In our series of polymers, M_n values were almost similar, but $Đ$ values greatly varied: 1.92, 4.33, 2.65, 3.87, and 3.18 for PBDTT, B70T30, B50T50, B30T70, and PBDTT-TPD, respectively (Table 1). We speculate that different $Đ$ values do not play significant role in our system since there is no correlation between $Đ$ and photovoltaic performance. For example, all random copolymers that have huge different $Đ$ values exhibit similar PCEs above 6.0%. However, in the case of PBDTT, poor photovoltaic performance might be attributed to low $Đ$.

We evaluated the charge carrier transport and recombination properties to investigate why random copolymers show better photovoltaic performance than PBDT-TPD. First, we measured the space charge limited current (SCLC) of hole-only devices (HODs) and electron-only devices (EODs) for pristine and blend films. The zero-field mobilities of electrons (μ_e) and holes (μ_h) are extracted from the *J*–*V* curves of the devices,[49] and the values are summarized in Table 2. The *J*–*V* curves are shown in Figure S11 (Supporting Information). The highest μ_h of 1.70×10^{-3} cm^2 V^{-1} s^{-1} was obtained from PBDTT-TPD, and PBDTT and all random copolymers exhibited moderate, similar μ_h of ≈10^{-4} cm^2 V^{-1} s^{-1}. This is because conjugated polymers consisting of random sequence usually have poor charge transport ability compared to regular structured polymers. In the case of HODs and EODs of blend films, μ_h values of all blend films decreased compared to pristine films, and all random copolymer blends exhibit similar mobilities: $\mu_e = 2.68 \times 10^{-6}$, 4.98×10^{-6}, 4.54×10^{-6} cm^2 V^{-1} s^{-1}, and μ_h of 2.36×10^{-6}, 1.33×10^{-6}, 2.40×10^{-6} cm^2 V^{-1} s^{-1} for B70T30, B50T50, and B30T70, respectively. However, the PBDTT-TPD blend has imbalanced charge carrier transport properties: μ_e is an order of magnitude higher than μ_h. This might be one of the reasons why PBDTT-TPD blend has poor photovoltaic performance.

The dependence of *J*–*V* characteristics on the light intensity was examined to obtain better insight into the charge carrier recombination of the devices.[50,51] Initially, the relationship between J_{SC} and light intensity can be described as $J_{SC} \propto I^S$. The J_{SC} was plotted against the light intensity on a logarithmic scale with the slope *S* of curves, as displayed in Figure 3c. A value of *S* close to unity represents the reduced bimolecular charge recombination. In addition, imbalanced charge carrier mobility also affects the S values by the build-up of space-charge in the devices.[52] Therefore, it is difficult to analyze the bimolecular recombination behavior from $J_{SC} \propto I^S$ when the devices show imbalanced charge carrier mobility. In our polymer blends, the calculated *S* values were similar: 0.95 for PBDTT and B70T30; 0.96, B50T50; 0.97, B30T70; and 0.96, PBDTT-TPD, respectively. Therefore, we conclude that all devices exhibit similar bimolecular recombination behaviors. Next, the dependence of V_{OC} on the light intensity was measured to assess the trap-assisted charge recombination processes.[53] The V_{OC} values logarithmically depend on light intensity with a slope of 1–2 with units of $k_B\ T\ q^{-1}$, where the slope close to 2 represents strong trap-assisted recombination in the OPV devices. In addition, if the surface recombination at active layers/contact interface exists, the slope can be reduced below $1\ k_B\ T\ q^{-1}$.[53] Therefore, the slope is determined by the combination of trap-assisted and surface recombination. The PBDTT, B70T30, B50T50, B30T70, and PBDTT-TPD devices yield values of 1.20, 1.16, 1.18, 1.09, and $1.31\ k_B T q^{-1}$, respectively (Figure 3d). All random copolymers have similar slope, while the highest slope is obtained from the PBDTT-TPD blend. This indicates that the PBDTT-TPD blend has the highest trap-assisted recombination by assuming that similar densities of surface recombination present in all devices. The low FF and J_{SC} of PBDTT-TPD can be attributed to high trap-assisted charge recombination and imbalanced μ_h/μ_e, although the polymer has a wide absorption range.

2.4. Structural and Morphological Properties

We performed grazing incidence X-ray scattering (GIXS) of the blends to analyze the polymer packing structures (Figure S12, Supporting Information). All polymer blends exhibited weak scattering peaks because the designed polymers have an amorphous nature, as discussed in the DSC. In accordance with a previous report, we did not obtain distinct π–π stacking peaks from PBDTT blend.[54] Random copolymers (B70T30–B30T70) and PBDTT-TPD containing TPD moiety also did not show noticeable π–π stacking peaks, which is in contrast to the previous literature: broad π–π stacking peaks were observed from PBDTT-TPD blend.[55] This might be due to the use of different acceptor materials and processing condition. Our system uses $PC_{71}BM$ as an acceptor and chlorobenzene for preparing blend solution, however in the literature, the PBDTT-TPD devices were optimized with $PC_{61}BM$ and chloroform solution. We guess that larger size of $PC_{71}BM$ may hinder the molecular organization of PBDTT-TPD during spin-coating process, and also different processing solvents can produce different packing structures and bulk heterojunction morphology. In this regard, all blend films showed similar scattering characteristics, i.e., (i) a prominent (100) peak from the lamellar stackings of polymer donors in the low *q* range (q = 0.25–0.35 Å^{-1}) and (ii) a broad amorphous halo from PCBM domains in the high *q* range (q = 1.2–1.5 Å^{-1}). The only noticeable change is a monotonic shift of the (100) lamel-

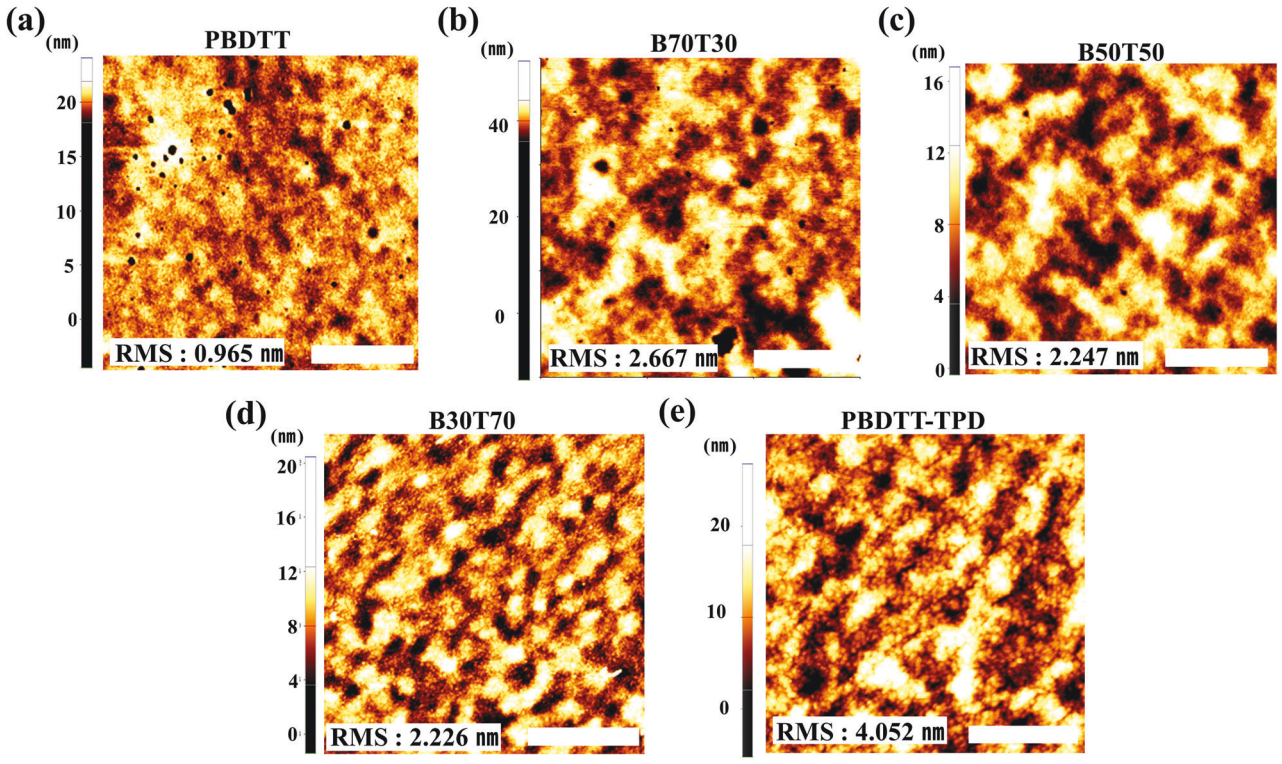

Figure 4. Tapping mode surface topographic atomic force microscopy (AFM) images of the donor:$PC_{71}BM$ blend films. The scale bar in the AFM images is 1 μm.

lar peaks toward the lower q from 0.35 $Å^{-1}$ (PBDTT) to 0.28 $Å^{-1}$ (PBDTT-TPD), which indicates a gradual increase in the lamellar spacings from 1.8 to 2.2 nm as an increasing fraction of TPD backbones in polymer donors. This result is consistent with our material design, given that the TPD building block has a long alkyl chain (octyl) compared to the PBDTT building block (2-ethylhexyl). PBDTT-based homo and random copolymers can be good model materials to investigate the importance of absorption properties for producing efficient IPVs by minimizing nanostructural and electrical properties.

Morphological changes in the donor:$PC_{71}BM$ blend films were measured using atomic force microscopy (AFM) (**Figure 4**). PBDTT blends show a very smooth film with distinct pinholes, which is the main reason for the decreased FF. Phase separation begins with increasing TPD content, and a coarse surface is observed in the PBDTT-TPD blend. The root-mean-squared (RMS) values of the PBDTT-TPD blend are significantly higher (4.052 nm) than those of PBDTT: 0.965 nm, B70T30: 2.667 nm, B50T50: 2.247 nm, and B30T70: 2.226 nm. From the GIXS study, we can conclude that nanostructures do not significantly influence the charge carrier transport and recombination properties of polymer blends. However, from the AFM analysis, the macroscopic morphology changes with or without the TPD unit. All random copolymers have similar morphologies with low RMS values; however, the PBDTT-TPD alternating copolymer has a high RMS value of 4.052 nm, which gives rise to poor J_{SC} and FF. We speculate that random sequence of BDTT and TPD in random copolymers hinders polymer assemblies during spin-coating process, resulting in enhanced miscibility with $PC_{71}BM$.

2.5. Photovoltaic Performance Under Indoor Light Sources

The indoor illumination conditions deviate substantially from those under AM 1.5G illumination conditions. Thus, the photovoltaic performance of the organic IPV device was evaluated under FL and LED light sources. Interestingly, organic IPVs with the random copolymer show a notable improvement in the photovoltaic performance under FL illumination conditions, as depicted in **Figure 5**a; the parameters are summarized in **Table 3** and Table S1 (Supporting Information). The best organic IPV devices with B30T70 exhibited the maximum PCE value of 18.3% with a V_{OC} of 0.74 V, J_{SC} of 112.3 μA cm^{-2}, and FF of 72.3% under FL 1000 lx illumination. In contrast, devices with PBDTT showed a considerably poor performance with a V_{OC} of 0.56 V, J_{SC} of 72.2 μA cm^{-2}, and FF of 53.1%, which results in a PCE of 6.6%. Similarly, devices with PBDTT-TPD exhibited a relatively low PCE of 14.6% under the same illumination conditions. The excellent photovoltaic performance of random copolymer devices can be attributed to the perfect spectral match of the absorption spectrum of the random copolymer with the irradiation spectrum of FL (Figure 2a). The absorption profile of B30T70 matches well with the emission of FL, and it justifies its excellent performance with high PCE and J_{SC} values under FL illumination. According to the equivalent-circuit diode model, J_{SC} and V_{OC} are linearly and logarithmically proportional to the light intensity, respectively.[1,51] Therefore, a linear decrease in J_{SC} values (from mA cm^{-2} to μA cm^{-2}) was expected as light intensities were varied from 100 mW cm^{-2} (AM 1.5G) to 0.33 mW cm^{-2} (FL 1000 lx). Similarly, a V_{OC} drop of 100–200 mV was estimated

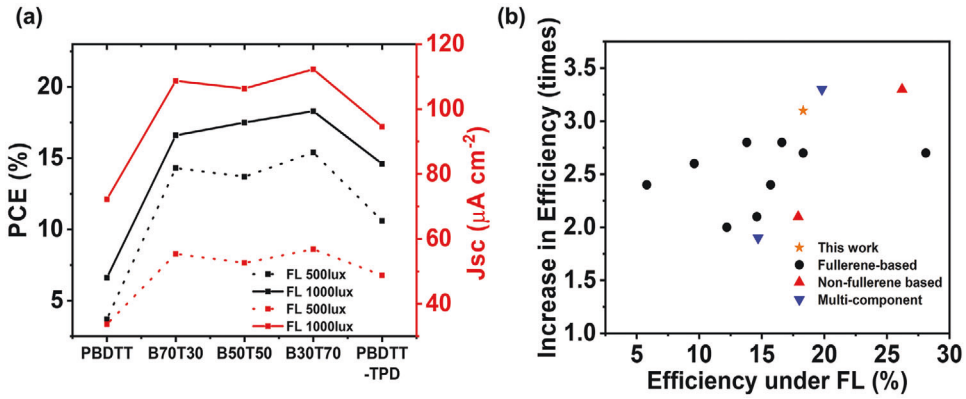

Figure 5. a) J_{SC} and power conversion efficiency (PCE) of devices under fluorescent lamp (FL) illumination. b) Comparison of PCE and increase in the PCE of indoor photovoltaics (IPVs) under FL illumination.

Table 3. Photovoltaic properties of BHJ photovoltaic cells under fluorescent lamp (FL) illuminations (500 lx: 0.19 μW cm^{-2} and 1000 lx: 0.33 μW cm^{-2}).

Active layer	Light source	V_{OC} [V]	J_{SC} [μA cm^{-2}]	FF [%]	PCE [%]	R_s [Ω cm^2]	R_{sh} [kΩ cm^2]
PBDTT	FL 500 lx	0.44 ± 0.04	33.7 ± 2.1	48.2 ± 1.2	3.7 ± 0.3	8.90	33.5
	FL 1000 lx	0.56 ± 0.01	72.2 ± 0.2	53.1 ± 0.8	6.6 ± 0.2	3.70	57.5
B70T30	FL 500 lx	0.70 ± 0.01	55.4 ± 0.6	70.6 ± 1.5	14.3 ± 0.2	9.26	247.3
	FL 1000 lx	0.73 ± 0.01	108.7 ± 1.0	70.4 ± 0.2	16.6 ± 0.2	8.59	173.9
B50T50	FL 500 lx	0.71 ± 0.02	52.6 ± 2.1	69.9 ± 1.7	13.7 ± 0.2	9.09	486.5
	FL 1000 lx	0.74 ± 0.02	106.3 ± 2.0	72.9 ± 0.4	17.5 ± 0.1	7.57	124.9
B30T70	FL 500 lx	0.73 ± 0.01	56.8 ± 0.5	71.4 ± 0.9	15.4 ± 0.1	9.10	165.3
	FL 1000 lx	0.74 ± 0.02	112.3 ± 0.9	72.3 ± 1.2	18.3 ± 0.1	9.17	118.9
PBDTT-TPD	FL 500 lx	0.73 ± 0.02	48.8 ± 1.1	56.7 ± 2.0	10.6 ± 0.1	11.01	290.8
	FL 1000 lx	0.77 ± 0.01	94.6 ± 0.5	66.7 ± 1.4	14.6 ± 0.4	12.15	77.8

under the same altered light conditions, and the reduction in V_{OC} values was as follows: PBDTT, 0.84 to 0.56 V; B70T30, 0.89 to 0.73 V; B50T50, 0.90 to 0.74 V; B30T70, 0.91 to 0.74; and PBDTT-TPD, 0.91 to 0.77V. The PBDTT devices observe a relatively significant drop in the V_{OC} that can be ascribed to the presence of high charge recombination that dominates under low-intensity light conditions.

The indoor performance of devices can be further validated by calculating the parasitic resistance values (R_s and R_{sh}) from the equivalent-circuit diode model.[51,56] Under indoor light conditions, which secure a large value of R_{sh} is essential, whereas the effect of R_s is insignificant because of extremely low-intensity light conditions.[56,57] The R_{sh} and R_s values of devices under FL 1000 lx were calculated as PBDTT: ≈57.5 kΩ cm^2 and ≈3.70 Ω cm^2; B70T30: ≈174 kΩ cm^2 and ≈8.6 Ω cm^2; B50T50: ≈125 kΩ cm^2 and ≈7.6 Ω cm^2; B30T70: ≈119 kΩ cm^2 and ≈9.17 Ω cm^2; and PBDTT-TPD: ≈78 kΩ cm^2 and ≈12.2 Ω cm^2. The significantly large R_{sh} values of the random copolymer over PBDTT and PBDTT-TPD devices justified their excellent performance under FL 1000 lx. However, the R_s value of PBDTT devices was smaller than that of the other devices. The effect of R_s does not critically affect indoor performance, as expected (Table 3). The *J–V* curves in the dark (Figure S10, Supporting Information) demonstrate that a small leakage current is associated with large R_{sh} values that contribute to enhancing the random copolymer organic IPV performance. For universal applicability, the device performance was examined under LED illumination conditions. The photovoltaic parameters under LED and FL follow a similar trend because the light intensities and spectra of indoor light sources (LED and FL) are considerably similar. The highest PCE of approximately 16.9% was achieved with B30T70 organic IPVs under 1000 lx LED, whereas the PBDTT and PBDTT-TPD exhibited PCE values of 7.1% and 11.2%, respectively. The photovoltaic performance of devices under LED illumination (500 and 1000 lx) is shown in Figure S13 (Supporting Information) and Table S2 (Supporting Information).

The IPV performance of random copolymer devices was compared with that of previously reported organic IPVs. For proper comparison, we collected the data measured under FL light source since different light sources significantly affect the performance of IPVs (Figure 5b and Table S3,).[1–3,13,14,31,58–61] Our device is not the best, but only three reports (CD1:PBN-10, PCDTBT:PDTSTPD:$PC_{71}BM$, and BTR:$PC_{71}BM$) show higher PCEs under FL than that of B30T70; among binary blend systems of polymer donor and fullerene-based IPVs, B30T70 blend has the best PCE. In addition, efficiency increments of B30T70 from 1-sun to indoor light conditions are very high compared with other high performance IPVs. This indicates that classical

wide bandgap polymers have a strong potential for indoor light energy harvesting applications, although they have poor performance under 1-sun conditions.

3. Conclusions

We successfully maximized the photovoltaic performance of organic IPVs by revisiting the classical PBDTT homopolymer and by straightforward random copolymerization using a TPD unit. The ratio of the TPD component in the random copolymer was varied to examine its effect on the optoelectrical, electrochemical, and morphological properties of organic IPVs. The optimized random copolymer (B30T70) exhibited a large PCE enhancement from 6.0% (AM 1.5G) to 18.3% (indoor light, FL 1000 lx). We mainly attribute the excellent IPV performance to the perfect spectral response of the B30T70 random copolymer with deep HOMO energy levels. Further, we found that the random copolymer showed balanced charge mobilities with suppressed trap-assisted recombination, which led to improved FF and J_{SC}. The proposed design strategies provide simple and easy molecular design guidelines for applications in organic IPVs by surveying and modifying classical photoactive materials that have a low profile because of their poor performance under 1-sun conditions.

4. Experimental Section

Materials: 2,6-Bis(trimethyltin)-4,8-bis(5-ethylhexyl-2-thienyl)benzo[1,2-b:4,5-b′]-dithiophene and 1,3-dibromo-5-octyl-4H-thieno[3,4-c]pyrrole-4,6(5H)-dione were purchased from Solarmer. 2,6- Dibromo-4,8-bis(5-(2-ethylhexyl)thiophen-2-yl)benzo[1,2-b:4,5-b']dithiophene was purchased from SunaTech, Inc. $PC_{71}BM$ was purchased from Brilliant Matter; all monomers were used without further purification.

Synthesis: Poly(4,8-bis(5-(2-ethylhexyl)thiophen-2-yl)benzo[1,2-b:4,5-b']dithiophene) (PBDTT): The polymer was synthesized by stille polycondensation based on a literature procedure.[34,38,39] In brief, 2,6-bis(trimethyltin)-4,8-bis(5-ethylhexyl-2-thienyl)benzo[1,2-b:4,5-b′]-dithiophene (0.98 eq, 0.1960 g, 0.217 mmol) and 2,6-dibromo-4,8-bis(5-(2-ethylhexyl)thiophen-2-yl)benzo[1,2-b:4,5-b']dithiophene (1 eq, 0.1629 g, 0.221 mmol) were dissolved in 10 mL degassed toluene. $Pd_2(dba)_3$ (0.02 eq) and tri(*o*-tolyl)phosphine (0.08 eq) were added to the mixture and stirred overnight at 100 °C. The resulting solution was precipitated into methanol. The Soxhlet extraction was performed successively with acetone, hexane, dichloromethane, and chlorobenzene to purify the polymer. The chlorobenzene fraction was collected for further characterization and device fabrication. Yield: 198 mg (77%); M_n = 16.6 kg mol^{-1}; and $Đ$ = 1.92. Elem. Anal. Calcd: C, 71.24; H, 7.15; S, 22.19%. Found: C, 70.0; H, 7.3; S, 21.8%.

Random copolymers (B70T30, B50T50, and B30T70) and PBDTT-TPD were synthesized by the Stille polycondensation described above. However, a toluene + DMF mixture was used as a solvent to obtain high-molecular weight polymers; the reaction was performed in a microwave reactor. In brief, 2,6-bis(trimethyltin)-4,8-bis(5-ethylhexyl-2-thienyl)benzo[1,2-b:4,5-b′]-dithiophene (1 eq), 2,6- dibromo-4,8-bis(5-(2-ethylhexyl)thiophen-2-yl)benzo[1,2-b:4,5-b']dithiophene (X eq), 1,3-dibromo-5-octyl-4H-thieno[3,4-c]pyrrole-4,6(5H)-dione (Y eq), $Pd_2(dba)_3$ (0.02 eq), and tri(*o*-tolyl)phosphine (0.08 eq) were dissolved in degassed toluene (0.04 M) and DMF (0.01 M). The solution was reacted at 100 °C for 5 h in a microwave reactor; the resulting solution was precipitated into methanol. The polymer was purified by Soxhlet extraction using acetone, hexane, and chloroform successively. The chloroform fraction was collected for further characterization and device fabrication.

Random copolymer B70T30: $X = 0.7$, $Y = 0.3$, Yield: 278 mg, (79%); M_n = 16.1 kg mol^{-1}; and $Đ$ = 4.33. Elem. Anal. Calcd: C, 70.66; H, 7.12; S, 21.24; N, 0.15; O, 1.14%. Found: C, 68.9; H, 7.2; S, 20.9; N, 0.4; O, 1.8%.

Random copolymer B50T50: $X = 0.5$, $Y = 0.5$, Yield: 245 mg, (74%); M_n = 16.9 kg mol^{-1}; and $Đ$ = 2.65. Elem. Anal. Calcd: C, 69.56; H, 7.11; S, 20.61; N, 0.83; O, 1.9%. Found: C, 69.4; H, 7.5; S, 19.4; N, 0.7; O, 2.1%.

Random copolymer B30T70: $X = 0.3$, $Y = 0.7$, Yield: 291 mg, (94%); M_n = 16.9 kg mol^{-1}; and $Đ$ = 3.87. Elem. Anal. Calcd: C, 69.11; H, 7.09; S, 19.98; N, 1.16; O, 2.66%. Found: C, 67.9; H, 7.0; S, 19.8; N, 1.0; O, 3.0%.

PBDTT-TPD: $X = 0$, $Y = 1$, Yield: 176 mg, (95%); M_n = 14.8 kg mol^{-1}; and $Đ$ = 3.18. Elem. Anal. Calcd: C, 68.45; H, 7.06; S, 19.03; N, 1.66; O, 3.80%. Found: C, 68.6; H, 7.0; S, 19.7; N, 1.6; O, 3.9%.

Characterization: ^{1}H NMR (Bruker, AVANCE III 400 MHz) spectra were acquired with *o*-dichlorobenzene-d4 as the solvent and tetramethylsilane (TMS) as the internal standard. The M_n and $Đ$ of polymers were determined based on a previous report.[34] The compositions of polymers were determined by elemental analysis with a Thermo Scientific Flash 2000 Series instrument. Decomposition temperatures were obtained from the TGA using TA Instruments Q500 under a nitrogen atmosphere at a heating rate of 10 °C min^{-1} from 30 °C to 600 °C. The DSC measurements were performed using a TA Instruments model NETZSCH at a heating and cooling rate of 10 °C min^{-1} under a nitrogen atmosphere. UV-vis absorption spectra were measured using a UV-1900 (Shimadzu). Electrochemical CV was conducted using WisEIS-1200Premium (Wizmac), and the detailed procedure is described in a previous report.[62] The HOMO and LUMO energy levels of polymers were estimated using empirical equation: $E_{HOMO} = (-4.80 + E_{1/2}(\text{ferrocene}) - E_{onset})$ eV and $E_{LUMO} = E_{HOMO} + E_g^{opt}$. AFM images were obtained using the Park SYSTEMS model XE-100 in the tapping mode. GIXS experiments were conducted at the dual source and environmental X-ray scattering (DEXS) facility operated by the Laboratory for Research on the Structure of Matter at the University of Pennsylvania (a Xeuss 2.0 system (Xenocs) using GeniX3D). A Cu source (λ = 1.54 Å) was used, and the sample-to-detector distance was 182 mm. The critical angle measured for the blended films was 0.2°. The hole and electron mobilities were measured by the SCLC model using ITO/MoOx/polymer blends/MoOx/Ag and ITO/ZnO/polymer blend/Al devices, respectively.[49] Current–voltage measurements in the range of 0–10 V were obtained, and the results were fitted to a space-charge limited function. The SCLC is described by

$$J_{SCLC} = \frac{9}{8}\varepsilon\varepsilon_0\mu\frac{V^2}{L^3}\cdot\exp\left(0.89\gamma\sqrt{\frac{V}{L}}\right) \quad (1)$$

where ϵ_0, ϵ, μ, V, L, and γ represent the permittivity of free space (8.85 × 10^{-14} F cm^{-1}), relative dielectric constant of the active layer (=3), mobility of charge carriers, potential across the device ($V = V_{applied} - V_{bi} - V_r$), active layer thickness, and field-activation factor, respectively. The active area of the SCLC devices was 0.168 cm^2.

Device Fabrication: For device fabrication, ITO-patterned glass (AMG, Korea) substrates were washed with a detergent (Liqui-Nox Phosphate-Free Liquid Detergent, Alconox, Inc., White Plains, NY, USA) in an ultrasonicator for 20 min and rinsed with deionized (DI) water. The substrates were cleaned with DI water, acetone, and isopropyl alcohol (IPA) sequentially on a sonicator bath for 20 min each and then dried with a nitrogen air blower. The ZnO layer was deposited by spin coating at 5000 rpm for 60 s, followed by thermal annealing at 200 °C for 30 min. The PEIE layer was then deposited using a 0.2-µm-thick PTFE filter at a spin speed of 5000 rpm for 60 s, which is followed by annealing at 110 °C for 10 min in the ambient air. The samples were loaded into a nitrogen-filled glove box for the photoactive layer. A solution of photoactive layer materials with a total concentration of 25 mg mL^{-1} was prepared in chlorobenzene with 3 vol% 1,8-diiodooctane (DIO) with a weight ratio of 1:2 (D:A) and stirred at a temperature of 45 °C for 1 h. Then, the photoactive layer was deposited at a spin speed of 1000 rpm for 60 s using a 0.45 µm PTFE filter. No thermal treatment was applied to the photoactive layer. Finally, a hole transport layer (HTL) MoO_X (10 nm) and top electrode, Ag (150 nm), were deposited using a shadow mask at a base pressure of ≈5.1 × 10^{-8} Torr

in a thermal evaporator system (Daedong High Tech, Republic of Korea) connected to a nitrogen-filled glove box.

Device Characterization: The *J–V* characteristic curves under simulated 1-sun illumination (AM 1.5G, McScience, Suwon, Republic of Korea) were measured using a source meter (2401; Keithley Instruments, Cleveland, OH, USA) controlled by a K730 program (McScience, Republic of Korea). For the indoor light characterizations of organic IPV devices, three artificial indoor light sources were used: an LED lamp (McScience, Suwon, Republic of Korea) with an irradiance of 0.17 mW cm^{-2} at 500 lx and 0.28 mW cm^{-2} at 1000 lx; an FL with an irradiance of 0.19 mW cm^{-2} at 500 lx, and 0.33 mW cm^{-2} at 1000 lx. A Slidac voltage regulator (SD-1000; DSELECTRON, Republic of Korea) was employed to regulate the light intensities of the indoor light sources. The irradiance values of the indoor light sources were measured experimentally using equipment (PMD100D, THORLABS). For that, lux meter was put below the light source and connected to the equipment (TES 1330A). Then, related illuminance and irradiance values were recorded. The EQEs of the devices were measured using an incident photon-to-current efficiency (IPCE) system (ORIEL IQE 200 System; Irvine Newport, CA, USA). The active area of the OPV devices was measured to be approximately 0.1 cm^2 using an optical microscope. The thickness of the photoactive layers was estimated to be 80, 95, 100, 85, and 95 nm for PBDTT, B70T30, B50T50, B30T70, and PBDTT-TPD, respectively.

Supporting Information

Supporting Information is available from the Wiley Online Library or from the author.

Acknowledgements

J.K. and M.A.S. contributed equally to this work. This work was supported by the Basic Science Research Program through the National Research Foundation of Korea (NRF), funded by the Ministry of Education (NRF-2020R1I1A306779). This work was also supported by the NRF grant funded by the Korea government (MSIT) (2022R1A2C2009523, 2019R1A6A1A11044070). C.L. acknowledges the use of the Dual Source and Environmental X-ray scattering facility operated by the Laboratory for Research on the Structure of Matter at the University of Pennsylvania (NSF MRSEC 17- 20530).

Conflict of Interest

The authors declare no conflict of interest.

Data Availability Statement

The data that support the findings of this study are available from the corresponding author upon reasonable request.

Keywords

control of absorption range, indoor photovoltaics, organic photovoltaics, random copolymers, wide-bandgap polymers

Received: March 26, 2022
Revised: April 29, 2022
Published online:

[1] H. Yin, J. K. W. Ho, S. H. Cheung, R. J. Yan, K. L. Chiu, X. Hao, S. K. So, *J. Mater. Chem. A.* **2018**, *6*, 8579.
[2] Y. You, C. E. Song, Q. V. Hoang, Y. Kang, J. S. Goo, D. Ko, J. Lee, W. S. Shin, J. W. Shim, *Adv. Funct. Mater.* **2019**, *29*, 1901171.
[3] H. S. Ryu, S. Y. Park, T. H. Lee, J. Y. Kim, H. Y. Woo, *Nanoscale* **2020**, *12*, 5792.
[4] H. Ryu, J. Lee, T. Kim, U. Khan, J. H. Lee, S. S. Kwak, H. Yoon, S. Kim, *Adv. Energy Mater.* **2017**, *7*, 1700289.
[5] F. Mo, Z. Chen, G. Liang, D. Wang, Y. Zhao, H. Li, B. Dong, C. Zhi, *Adv. Energy Mater.* **2021**, *11*, 2000035.
[6] Z. Wu, T. Cheng, Z. L. Wang, *Sensors* **2020**, *20*, 2925.
[7] J. W. Matiko, N. J. Grabham, S. P. Beeby, M. J. Tudor, *Meas. Sci. Technol.* **2013**, *25*, 012002.
[8] L. Atzori, A. Iera, G. Morabito, *Comput. Networks* **2010**, *54*, 2787.
[9] A. Al-Fuqaha, M. Guizani, M. Mohammadi, M. Aledhari, M. Ayyash, *IEEE Commun. Surv. Tutorials* **2015**, *17*, 2347.
[10] J. Huang, A. Karki, V. V. Brus, Y. Hu, H. Phan, A. T. Lill, M. Wang, G. C. Bazan, T. Nguyen, *Adv. Mater.* **2018**, *30*, 1804794.
[11] C. L. Cutting, M. Bag, D. Venkataraman, *J. Mater. Chem. C* **2016**, *4*, 10367.
[12] R. Cheng, C. Chung, H. Zhang, F. Liu, W. Wang, Z. Zhou, S. Wang, A. B. Djurišić, S. Feng, *Adv. Energy Mater.* **2019**, *9*, 1901980.
[13] H. K. H. Lee, Z. Li, J. R. Durrant, W. C. Tsoi, *Appl. Phys. Lett.* **2016**, *108*, 253301.
[14] H. K. H. Lee, J. Wu, J. Barbé, S. M. Jain, S. Wood, E. M. Speller, Z. Li, F. A. Castro, J. R. Durrant, W. C. Tsoi, *J. Mater. Chem. A* **2018**, *6*, 5618.
[15] H. Yin, J. K. W. Ho, V. Piradi, S. Chen, X. Zhu, S. K. So, *Small Methods* **2020**, *4*, 2000136.
[16] M. A. Saeed, S. Cheng, S. Biswas, S. H. Kim, S. Kwon, H. Kim, Y. Kim, J. W. Shim, *J. Power Sources* **2022**, *518*, 230782.
[17] L. Ma, Y. Chen, P. C. Y. Chow, G. Zhang, J. Huang, C. Ma, J. Zhang, H. Yin, A. M. Hong Cheung, K. S. Wong, S. K. So, H. Yan, *Joule* **2020**, *4*, 1486.
[18] A. Wadsworth, M. Moser, A. Marks, M. S. Little, N. Gasparini, C. J. Brabec, D. Baran, I. McCulloch, *Chem. Soc. Rev.* **2019**, *48*, 1596.
[19] X. Wang, Q. Sun, J. Gao, J. Wang, C. Xu, X. Ma, F. Zhang, *Energies* **2021**, *14*, 4200.
[20] Y. Zeng, D. Li, H. Wu, Z. Chen, S. Leng, T. Hao, S. Xiong, Q. Xue, Z. Ma, H. Zhu, Q. Bao, *Adv. Funct. Mater.* **2022**, *32*, 2110743.
[21] S. Karuthedath, J. Gorenflot, Y. Firdaus, N. Chaturvedi, C. S. P. De Castro, G. T. Harrison, J. I. Khan, A. Markina, A. H. Balawi, T. A. D. Peña, W. Liu, R. Liang, A. Sharma, S. H. K. Paleti, W. Zhang, Y. Lin, E. Alarousu, S. Lopatin, D. H. Anjum, P. M. Beaujuge, S. De Wolf, I. Mcculloch, T. D. Anthopoulos, D. Baran, D. Andrienko, F. Laquai, *Nat. Mater.* **2021**, *20*, 378.
[22] Q. He, W. Sheng, M. Zhang, G. Xu, P. Zhu, H. Zhang, Z. Yao, F. Gao, F. Liu, X. Liao, Y. Chen, *Adv. Energy Mater.* **2021**, *11*, 2003390.
[23] W. Lee, S. Jeong, C. Lee, G. Han, C. Cho, J. Lee, B. J. Kim, *Adv. Energy Mater.* **2017**, *7*, 1602812.
[24] G. Li, R. Zhu, Y. Yang, *Nat. Photonics.* **2012**, *6*, 153.
[25] X. Ma, A. Zeng, J. Gao, Z. Hu, C. Xu, J. H. Son, S. Y. Jeong, C. Zhang, M. Li, K. Wang, H. Yan, Z. Ma, Y. Wang, H. Y. Woo, F. Zhang, *Natl. Sci. Rev.* **2021**, *8*, 305.
[26] R. Sun, W. Wang, H. Yu, Z. Chen, X. Xia, H. Shen, J. Guo, M. Shi, Y. Zheng, Y. Wu, W. Yang, T. Wang, Q. Wu, Y. Yang, X. Lu, J. Xia, C. J. Brabec, H. Yan, Y. Li, J. Min, *Joule* **2021**, *5*, 1548.
[27] J. Yuan, Y. Zhang, L. Zhou, G. Zhang, H. Yip, T. Lau, X. Lu, C. Zhu, H. Peng, P. A. Johnson, M. Leclerc, Y. Cao, J. Ulanski, Y. Li, Y. Zou, *Joule* **2019**, *3*, 1140.
[28] R. Ma, T. Liu, Z. Luo, Q. Guo, Y. Xiao, Y. Chen, X. Li, S. Luo, X. Lu, M. Zhang, Y. Li, H. Yan, *Sci. China Chem.* **2020**, *63*, 325.
[29] Y. Lin, Y. Firdaus, F. H. Isikgor, M. I. Nugraha, E. Yengel, G. T. Harrison, R. Hallani, A. El-Labban, H. Faber, C. Ma, X. Zheng, A. Subbiah, C. T. Howells, O. M. Bakr, I. McCulloch, S. D. Wolf, L. Tsetseris, T. D. Anthopoulos, *ACS Energy Lett.* **2020**, *5*, 2935.
[30] Y. Cui, Y. Wang, J. Bergqvist, H. Yao, Y. Xu, B. Gao, C. Yang, S. Zhang, O. Inganäs, F. Gao, J. Hou, *Nat. Energy* **2019**, *4*, 768.

[31] Z. Ding, R. Zhao, Y. Yu, J. Liu, *J. Mater. Chem. A* **2019**, *7*, 26533.
[32] Y. Cui, H. Yao, T. Zhang, L. Hong, B. Gao, K. Xian, J. Qin, J. Hou, *Adv. Mater.* **2019**, *31*, 1904512.
[33] J. K. W. Ho, H. Yin, S. K. So, *J. Mater. Chem. A* **2020**, *8*, 1717.
[34] T. E. Kang, T. Kim, C. Wang, S. Yoo, B. J. Kim, *Chem. Mater.* **2015**, *27*, 2653.
[35] J. Kim, J. B. Park, S. C. Yoon, I. H. Jung, D. Hwang, *J. Mater. Chem. C* **2016**, *4*, 217.
[36] B. Zhao, H. Wu, W. Wang, H. Liu, J. Liu, Z. Cong, C. Gao, *React. Funct. Polym.* **2019**, *145*, 104378.
[37] J. Kim, J. B. Park, F. Xu, D. Kim, J. Kwak, A. C. Grimsdale, D. Hwang, *Energy Environ. Sci.* **2014**, *7*, 4118.
[38] J. Yuan, Z. Zhai, H. Dong, J. Li, Z. Jiang, Y. Li, W. Ma, *Adv. Funct. Mater.* **2013**, *23*, 885.
[39] H. D. Magurudeniya, R. S. Kularatne, E. A. Rainbolt, M. P. Bhatt, J. W. Murphy, E. E. Sheina, B. E. Gnade, M. C. Biewer, M. C. Stefan, *J. Mater. Chem. A* **2014**, *2*, 8773.
[40] Y. Su, Y. Lin, K. Wei, *J. Mater. Chem. A* **2017**, *5*, 24051.
[41] T. E. Kang, J. Choi, H. Cho, S. C. Yoon, B. J. Kim, *Macromolecules* **2016**, *49*, 2096.
[42] M. Scharber, D. Mühlbacher, M. Koppe, P. Denk, C. Waldauf, A. Heeger, C. Brabec, *Adv. Mater.* **2006**, *18*, 789.
[43] J. Brédas, D. Beljonne, V. Coropceanu, J. Cornil, *Chem. Rev.* **2004**, *104*, 4971.
[44] A. Sacramento, M. Ramírez-Como, V. S. Balderrama, J. G. Sánchez, J. Pallarès, L. F. Marsal, M. Estrada, *J. Mater. Chem. C* **2021**, *9*, 6518.
[45] M. Jørgensen, K. Norrman, F. C. Krebs, *Sol. Energy* **2008**, *92*, 686.
[46] M. Shi, T. Wang, Y. Wu, R. Sun, W. Wang, J. Guo, Q. Wu, W. Yang, J. Min, *Adv. Energy Mater.* **2021**, *11*, 2002709.
[47] H. Kang, M. A. Uddin, C. Lee, K. Kim, T. L. Nguyen, W. Lee, Y. Li, C. Wang, H. Y. Woo, B. J. Kim, *J. Am. Chem. Soc.* **2015**, *137*, 2359.
[48] C. Liu, K. Wang, X. Hu, Y. Yang, C. Hsu, W. Zhang, S. Xiao, X. Gong, Y. Cao, *ACS Appl. Mater. Interfaces* **2013**, *5*, 12163.
[49] T. P. A. Van Der Pol, J. Li, B. T. Van Gorkom, F. J. M. Colberts, M. M. Wienk, R. A. J. Janssen, *J. Phys. Chem. C* **2021**, *125*, 5505.
[50] W. Shockley, W. T. Read, JR., *Phys. Rev.* **1952**, *87*, 835.
[51] S. R. Cowan, A. Roy, A. J. Heeger, *Phys. Rev.* **2010**, *82*, 245207.
[52] L. J. A. Koster, V. D. Mihailetchi, H. Xie, P. W. M. Blom, *Appl. Phys. Lett.* **2005**, *87*.
[53] V. V. Brus, *Org. Electron.* **2016**, *29*, 1.
[54] T. E. Kang, H. Cho, H. J. Kim, W. Lee, H. Kang, B. J. Kim, *Macromolecules* **2013**, *46*, 6806.
[55] T. Kim, J. Kim, T. E. Kang, C. Lee, H. Kang, M. Shin, C. Wang, B. Ma, U. Jeong, T. Kim, B. J. Kim, *Nat. Commun.* **2015**, *6*, 8547.
[56] R. Steim, T. Ameri, P. Schilinsky, C. Waldauf, G. Dennler, M. Scharber, C. J. Brabec, *Sol. Energy* **2011**, *95*, 3256.
[57] S. Y. Park, Y. Li, J. Kim, T. H. Lee, B. Walker, H. Y. Woo, J. Y. Kim, *ACS Appl. Mater. Interfaces* **2018**, *10*, 3885.
[58] M. A. Saeed, S. H. Kim, H. Kim, J. Liang, H. Y. Woo, T. G. Kim, H. Yan, J. W. Shim, *Adv. Energy Mater.* **2021**, *11*, 2003103.
[59] C. Chen, H. Ting, Y. Li, Y. Lo, P. Sher, J. Wang, T. Chiu, C. Lin, I. Hsu, J. Lee, S. Liu, K. Wong, *ACS Appl. Mater. Interfaces* **2019**, *11*, 8337.
[60] S. Yang, Z. Hsieh, M. L. Keshtov, G. D. Sharma, F. Chen, *Sol. RRL* **2017**, *1*, 1700174.
[61] M. Nam, H. Y. Noh, J. Kang, J. Cho, B. K. Min, J. W. Shim, D. Ko, *Nano Energy* **2019**, *58*, 652.
[62] C. Lee, H. Kang, W. Lee, T. Kim, K. Kim, H. Y. Woo, C. Wang, B. J. Kim, *Adv. Mater.* **2015**, *27*, 2466.